

Student Name: Jason Nishiyama

HET615

Student ID: 6690025

Instructor: Mel Hulbert

## SAO Essay Cover Page

### Filtering the Sky

All of the work contained in this essay is my own original work, unless otherwise clearly stated and referenced.

I have read and understood the SAO Plagiarism Page “What is Plagiarism and How to Avoid It” at <http://astronomy.swin.edu.au/sao/students/plagiarism/>

## Abstract

We present a method of performing searches for elemental emission lines without the use of spectroscopy. Through the use of a combination of wide and narrow band filters and a standard astronomical CCD imager, the detection of specific emission lines can be performed. This could result in possible cost and time savings over spectroscopic methods. A method of narrow band filter synthesis is also presented as a method of detecting emission lines for which a specific filter is unavailable.

## 1. Introduction

Filters have been used by professional astronomers for over 100 years to enhance observations (Wallace 1908). Gelatin filters were originally used to correct the chromatic aberration present in the refracting telescopes of the day (Wallace 1906). Later professional astronomers have used filters to identify colour in astronomical objects through the generation of colour indexes (Maitzen 1976) or for searches for particular elements in an object (Forde et al 2005).

Amateurs astronomers have also used filters to better enable visual observations of planets and other extended objects by enhancing the contrast of features on the planets and objects. Since the 1970's narrow band filters have been available to amateur astronomers who have used them to help combat light pollution during visual observation (Dickenson & Dyer 2002).

### 1.1. Filters

In general filters can be organized by their bandwidth, that is how much of the electromagnetic spectrum they allow to pass through. Wide band filters allow a comparatively large portion of the light that falls upon them through. These allow either a whole part of the spectrum through, for example all visible light; or a large part of a section of the spectrum through such as blue or green light. Narrow band filters allow much less of the light through. These are usually made to allow only the light from one particular emission line or two adjacent lines through. This allows the study of an object in the light from a particular element or to view an object in light polluted skies by blocking the light from other sources.

Filters can also be organized based on their method of manufacture. Dye filters and dichroic filters are the two basic types. Each will be discussed below.

### 1.1.1. *Dye filters*

Dye filters were the first to be developed, manufactured and used in astronomical observations (Wallace 1908). Dye filters work on a very simple principle in that the dye coating absorbs some wavelengths of light while allowing others to pass. What gets absorbed and what gets passed depends on the colour properties of the dye which in turn is determined by the chemical properties of the dye (Mees & Wratten 1906). Changing the chemicals in the dye changes the colour.

Early filters were often made at the observatory as they were needed. These were made using gelatin as a carrier for the dyes which was then suspended in front of the film at the end of the telescope (Wallace 1906). This was a difficult process with careful measurement needed to ensure consistent results in the filter's transmission profile, that is what light was desired to be allowed through the filter. Also the optical qualities of the gelatin and hence the filter would change as the gel dried (von Hubl 1912) and this also had to be accounted for. Eventually consistent quality, commercially produced filters became available and dye filters became commonplace in astronomy. Dye filters became so ubiquitous that when Johnson developed his UBV photometric system, he was able to specify very specific commercially available dye filters from Corning (Johnson 1955). Dye filters are still common in amateur astronomical use for visual observing as they are quite inexpensive in comparison to dichroic filters. This is due to the simplicity of constructing dye filters which basically is sandwiching the dye carrier between two pieces of optical glass.

This is the primary advantage of dye filters, their cost. Their extensive use outside of astronomy and simplicity of manufacture means that economies of scale can drive down unit cost. Due to their use in photography there is also a very wide range of colour bands for these filters that can be specified by simply ordering a specific Wratten number (Peed 1987).

A significant disadvantage of dye filters is their tendency to fade over time (Peed 1987; OptosigmaWeb 2011). This fading will cause the filter's transmission profile to change from the standard expected by the user. For amateurs making visual observations this fading would not be as large a problem as the change is slow over time and would be difficult to detect visually. For anyone using dye filters for photometric work, this fading must be taken into consideration as unwanted light will be allowed through a faded filter, contaminating the data.

Another disadvantage of dye filters is the difficulty in making very narrow band filters with this construction method. The narrowest Wratten filters available, such as #73, have a bandwidth of about 60nm (Peed 1987), and at that transmitting only 4.5% of the light at the centre of the bandpass. This makes using dye filters difficult for emission line observation as some emission lines are quite close together, such as H $\gamma$  and [OIII] which are only 25nm apart (Crockett et al 2006). The very limited amount of light that passes through these narrow dye filters also means longer exposure times at the telescope

to compensate for the loss of light due to absorption in the filter. Further many dye filters have unwanted infrared band passes over and above their desired bandpass (Peed 1987). This requires IR cut-off filters when using modern detectors such as CCDs which can be sensitive to infrared light.

A final disadvantage to this type of filter is that as it absorbs the light it is blocking, it can warm up as the energy from the light is absorbed by the dye. This is not a great disadvantage in astronomical situations since, with the possible exception of solar astronomy, the amount of light passing through the filter is very low.

### 1.1.2. *Dichroic filters*

Dichroic or interference filters work in a different way. In essence they work in the same manner as Fabry-Perot interferometers (Lissberger 1959). In a Fabry-Perot interferometer, two glass plates are placed very close together. As light passes through the plates, constructive and destructive interference caused as the light bounces back and forth between the plates allows some wavelengths light to pass through while reflecting all other wavelengths light back out of the interferometer (Fabry & Perot 1901). Dichroic filters work in the same manner except instead of two plates, it is thin films that act as the interferometer Lissberger (1959). Various thicknesses and numbers of these thin films are evaporated onto the substrate material until the desired number and thicknesses are achieved.

Dichroic filters are also not a new idea. With the development of the Fabry-Perot interferometer in the late 1890's it was only 40 years later in 1939 when it was suggested that dichroic filters could be used in astronomy (Johnson 1939). By the 1970's the use of dichroic filters was so wide spread that this type of filter had even entered the amateur market (Dickenson & Dyer 2002). They are now so ubiquitous that they are displacing dye filters in non-scientific applications, especially those where heat retention is an issue (OptosigmaWeb 2011). In fact all the filters used in this survey, both wide and narrow band are dichroic filters.

The primary advantage of dichroic filters is the ability to design the layers in such a way as to create virtually any transmission profile needed for a particular task. Through some complicated mathematics, it is possible to work out what light will get through a dichroic filter before it is even made (Lissberger 1959). This is in contrast to dye filters the early use of which was marked by much trial and error to get the desired bandpass (Mees & Wratten 1906; Wallace 1906).

This ability to be designed and manufactured with high precision means that dichroic filters can be made with band passes as low as a few nanometres. The relatively inexpensive consumer grade dichroic filters used in this survey, shown in Table 1, have band passes as

low as  $\sim 10\text{nm}$ . Other commercially available consumer grade filters can be much narrower. Unlike narrow band dye filters, narrow band dichroic filters allow upwards of 90% of the light in the desired band through while blocking out all other wavelengths (Orion Telescopes 2009ab). Generally with properly designed dichroic filters infrared cut-off filters are not even required.

As the dichroic filters block the unwanted frequencies by reflecting them back out of the filter, very little if any of the unwanted light is absorbed by the filter which resolves the heating issues that exist in dye filters. More importantly since dyes are not used, fading is no longer an issue (OptosigmaWeb 2011). This makes dichroic filters well suited for photometry as little if any change to the expected transmission profile will occur to the filter over time.

Dichroic filters are not perfect however. There are a few disadvantages to this type of filter that do not exist with dye filters. The first of which comes from the main strength of this type of filter, the ability to design for the filter's bandpass. The mathematics to design a particular dichroic filter is quite involved requiring many calculations which prior to high speed electronic computers would have had to be done manually (Caballero 1947; Lissberger 1959; Lissberger & Wilcock 1959).

With difficulty of design often comes difficulty of construction. Dichroic filters require more precision required to construct than is needed for a dye filter as many extremely thin layers of film must be precisely placed on the filter's substrate in order to have the proper transmission profile. This makes this type of filter much more expensive than dye filters to construct and hence to purchase. As an example the author has several dye type filters for both astronomical and terrestrial photographic work, none of which cost more than \$20 to purchase. The narrow band dichroic filters used in this survey were in the \$100 range and that was at a discount. More precision sometimes equals more cost.

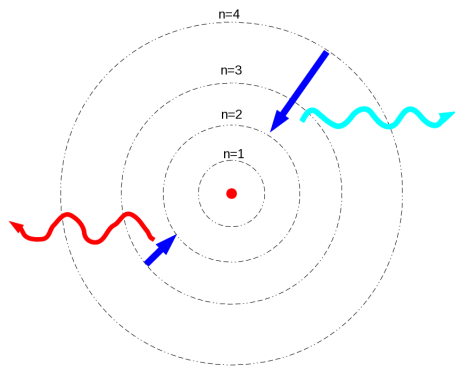
Due to the way dichroic filters work, it is also imperative that the light enter the filter at the normal, that is perpendicular to the plane of the filter. Tilting the filter will, in essence, change the thickness of the filter layers and hence the transmission profile of the filter. Thus it is very important that the filter be held securely in front of and parallel to the imager. Some researchers have taken this undesirable effect of tilted dichroic filters and turned it into a method of having a variable wavelength narrow band filter. Knowing how this effect works allows for a new bandpass to be calculated ahead of time and the filter set to the appropriate angle to pass the desired wavelength (Lofdahl et al 2011). This property, properly used, can result in considerable cost savings if one wishes to observe wavelengths very close to the design bandpass of the filter.

Temperature also affects this type of filter. Significant changes in temperature can significantly change the wavelengths transmitted through a dichroic filter (Cianci et al 2004). This is due to the changing temperature changing the index of refraction of the various layers that make up the filter. This is a concern for professional astronomers who

may take a filter and cool it significantly to ensure it will not emit in the infrared for infrared observations. As such filters that are to be cooled, especially narrow band filters where any significant change in bandpass may take the filter off the desired emission line, must be designed with cooling in mind.

## 1.2. Detecting Elements With Filters

It is amazing that we can detect the chemical make up of objects at great distance. This is possible because of the way that matter interacts with electromagnetic radiation such as visible light. Inside an atom the electrons move around the nucleus in very specific shells based on the energy of the electron. Now the electron can only have certain energies and hence only certain shells can exist. Also electrons prefer to be in the lowest energy state they can be, which means giving up energy as a photon to do this. Since the electrons can only be in certain energy states, to go from one to the other a very specific amount of energy must be released. This quantization of energy means that only photons of certain energies and hence wavelengths can be produced by electrons moving to lower energy shells (Hyperweb 2011a; Halliday & Resnick 1988, p 165). For example in the hydrogen atom an electron moving from shell 3 to shell 2 produces a photon at a wavelength of about 656 nm producing the  $H\alpha$  line whereas a transition from shell 4 to shell 2 produces a photon of about 486 nm producing the  $H\beta$  line Hyperweb (2011b) as in Figure 1. Conversely, an  $H\alpha$  photon can be absorbed by a hydrogen atom that has its electron in shell 2 and use that energy to boost the electron to shell three. In this case the photon is absorbed.



$H\alpha$  transition (red) and  $H\beta$  Transition (Blue)

Fig. 1.— Hydrogen electron transitions

Now hot objects will emit as a black body, that is producing a continuous spectrum as in the top of Figure 2. If a cooler cloud of material is between the observer and a hot object, the atoms in the cloud will absorb photons based on the transitions permitted in the

particular atoms and molecules in the cloud. Since the photons are re-emitted in a random direction, very few arrive at the observer and thus a dark absorption spectrum is created like the middle of Figure 2. Finally a cloud that is having energy input from some object out of the line of site will produce an emission spectrum such as at the bottom of Figure 2 as it emits photons based on the electrons returning to lower energy levels. Since each element and molecule produce a unique set of lines, examining the spectra of an object can allow the observer to determine what species are present (Freedman & Kaufmann 2007, p 113).

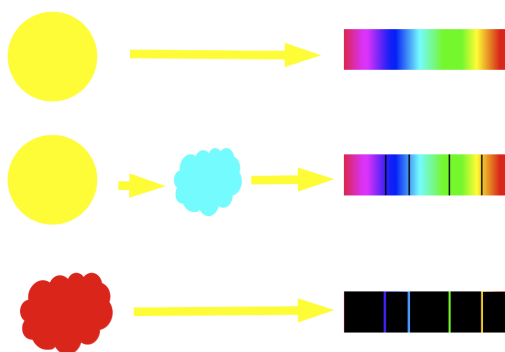


Fig. 2.— Spectrum types

Normally these spectra are observed with a spectrograph. A small slit is placed over the object so that only the light of the object of interest enters the spectrograph. These devices then spread the light from the object being observed out into a spectrum either with a prism, or more commonly a diffraction grating of some type. This spectrum is then recorded on a CCD or film for later analysis. Spectrographs are generally large, bulky and expensive pieces of equipment (Birney et al 2008, p 215) and even those aimed at the amateur market are bulky and expensive. For example one particular amateur spectrograph masses at 1.4kg which is a significant addition to a telescope that itself may only mass between 3 and 10kg. It also comes at a cost of over 2000 Euros, approximately \$2800 (ShelyakWeb 2011). One must also add to this the CCD imager which adds more mass and expense. For amateurs, this can be prohibitively expensive in terms of the device and the robust mount required to hold the spectrograph, the telescope and imager.

Compared to spectrographs filters are comparatively inexpensive, often in the \$100 to \$200 range. Many amateur astronomers may also already own a set of narrow band filters for use in observing in light polluted areas, for example the UHC filter used in this survey was purchased by the author to aid in observing from his suburban back yard. This further reduces the cost of starting such a survey for amateurs that wish to perform scientific observations. For professionals surveying for a particular element, spectroscopy means each

object must be observed separately. with a set of filters and large enough CCD imager, many objects may be observed at the same time, reducing time at the telescope. Since time at professional observatories is at a premium, anything that can reduce this observing time is useful.

By using narrow band filters that only pass the light of specific emission lines in combination with wider band filters it should be possible to detect the element line by a difference in the brightness from the emitting object compared to the change in brightness of a continuum source. If there is a significant difference in the change of brightness of the target object compared to the change in brightness of the continuum objects in the same field through the same set of filters, then this is likely due to the emission line being present. This is because the narrow band filter allows considerably less of the continuum light through, dropping the brightness of the continuum objects. The narrow band filter however does not cause the same drop in brightness for an object emitting the particular emission line as the brightness caused by the emission line is permitted to pass through the filter unimpeded causing less of a brightness reduction. This can be seen in Figure 3 where the amount of flux from the continuum object on the top is much less through the narrow band filter than through the wide band filter whereas the amount of flux for the emission line object stays relatively the same through both filters.

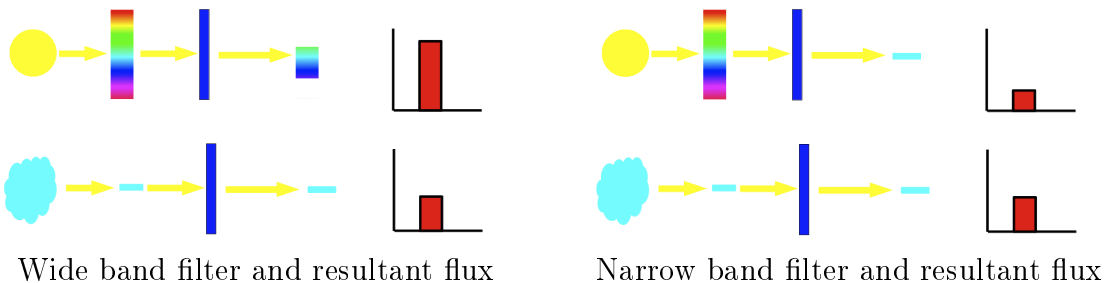


Fig. 3.— Comparison of continuum and line through wide and narrow filters

This is similar to techniques used in standard photometry where indexes are produced comparing the change in flux through various filters is used to find specific spectral features to locate objects such as peculiar stars. Much of this work uses observations performed with narrow band filters (Maitzen 1976; Paunzen et al 2002; Edwards et al 2010). Also survey work looking for specific object classes by looking for their emissions has also been performed with some success (Nago et al 2008). Belikov & Roser (2008) have used narrow band filters to estimate the astrophysical properties of stars. Finally Forde et al (2005) have attempted to determine the chemical composition of globular clusters using basically the same process as attempted in this survey.

## 2. Experimental Method

### 2.1. Equipment

This project used the 0.36m Schmidt-Cassegrain telescope (Celestron C-14) located at the Wilson Coulee Observatory. The observatory is located near Calgary, Alberta, Canada at  $50^d46^m21^s$  N,  $114^d01^m41^s$  W at an altitude of 1141 m. The telescope was equatorially mounted on a fork mount during the observations. A focal reducer was used to reduce the optical system from  $f$  11.2 to  $f$  7.3. This was done to enlarge the field of view of the optical system/imager combination.

The imager used was an Orion Star Shoot Deep Space Monochrome Imager III. This imager uses a front illuminated Sony ICX285AL CCD which is thermo electrically cooled to approximately  $30^{\circ}\text{C}$  below the ambient environmental temperature. The ICX285AL sensor is a  $1392 \times 1040$  array of  $6.45 \mu\text{m}$  pixels. With this CCD and optical system, a field of view of approximately  $12.2 \times 9.1$  arc minutes was possible.

A total of seven dichroic filters were used during observations. These are summarized in Table 1. It is important to note that the R, G and B filters are photographic band filters. They do not match the B, V and R filters of the Johnson system. In this paper the letters R, G and B will refer to the photographic bands unless otherwise mentioned. The filters were housed in a five filter magazine between the imager and the focal reducer. The OIII and SII filters were swapped with the UHC and B filters in the magazine as required during imaging.

Name	Width	$\lambda_{top}$ (nm)	$\lambda_{bottom}$ (nm)	Colour	Manufacturer	Ref
L	Wide	380	685	Full Spectrum	Orion	(1)
R	Wide	625	680	Red	Orion	(1)
G	Wide	480	560	Green	Orion	(1)
B	Wide	390	510	Blue	Orion	(1)
UHC	Narrow	480	515	Blue-Green	Antares	(2)
OIII	Narrow	490	510	Blue-Green	Orion	(3)
SII	Narrow	665	677	Deep Red	Orion	(4)

References:

(1) Orion Telescopes (2009); (2) Antares (2008); (3) Orion Telescopes (2009a); (4) Orion Telescopes (2009b)

Table 1: Program Filters

## 2.2. Target Objects

Six objects were selected for imaging. The criterion for object selection was based on the following: 1) target visible over the observing site during the program observation period; 2) objects to reflect a range of object categories, e.g. galaxy, emission nebula, etc.; 3) objects bright enough for short integration time imaging; and 4) object small enough for a majority of the object to fit inside the field of view of the imager/optical system combination. This resulted in the selection of one elliptical galaxy, one spiral galaxy, one globular cluster, one emission nebula and two planetary nebulae. The program objects are summarized in Table 2.

Object	RA (J2000)	Dec (J2000)	$m_B$	Type
NGC 185	00 <sup>h</sup> 38 <sup>m</sup> 57.9 <sup>s</sup>	+48 <sup>d</sup> 20 <sup>m</sup> 14.6 <sup>s</sup>	11.0	Elliptical Galaxy
NGC 598	01 <sup>h</sup> 33 <sup>m</sup> 50.9 <sup>s</sup>	+30 <sup>d</sup> 39 <sup>m</sup> 35.8 <sup>s</sup>	6.3	Spiral Galaxy
NGC 650	01 <sup>h</sup> 42 <sup>m</sup> 19.9 <sup>s</sup>	+51 <sup>d</sup> 34 <sup>m</sup> 31.2 <sup>s</sup>	16.1	Planetary Nebula
NGC 6618	18 <sup>h</sup> 20 <sup>m</sup> 26 <sup>s</sup>	–16 <sup>d</sup> 10 <sup>m</sup> 36 <sup>s</sup>	6.7	Emission Nebula
NGC 6838	19 <sup>h</sup> 53 <sup>m</sup> 46.5 <sup>s</sup>	+18 <sup>d</sup> 46 <sup>m</sup> 45.1 <sup>s</sup>	7.9	Globular Cluster
NGC 7662	23 <sup>h</sup> 25 <sup>m</sup> 53.6 <sup>s</sup>	+42 <sup>d</sup> 32 <sup>m</sup> 06 <sup>s</sup>	9.4	Planetary Nebula

Object data from SIMBAD.

Table 2: Program Objects

## 2.3. Observations

Observations were undertaken on separate 5 nights. Pilot observations were performed on 04 September 2011 with program observations performed on 10, 12, 14 and 21 October 2011. For the program images a series of seven images were taken of each object through each filter. The integration time of each image was 2 minutes. Dark frames as well as sky and dome flats were also taken.

A sticky spot on the worm gear that drives the telescope caused the frame to shift slightly every few minutes. The undesirable effect of this was that occasionally an image would need to be rejected due to the objects in the frame being smeared slightly. Since the telescope would not return to its original pointing after the drive error occurred, this inadvertently produced a desirable effect of locating the object on a slightly different portion of the CCD. This allowed for the object to be imaged on a different portion of the CCD helping to negate differences in individual pixels.

## 2.4. Data reduction

Images were examined manually to reject those with tracking errors. For each object and each filter set of seven images, four were selected. This produced a total of 28 images per object, four images for each of seven filters. These selected images were then dark and flat fielded in IRAF. Each four image set was then additively stacked using Maxim DL Essentials providing a total integration time per filter of 8 minutes. Further image registration was performed using the Iris software package to allow the subtraction of the OIII frames from the UHC frames. A synthetic hydrogen beta ( $H\beta$ ) frame was produced by subtracting the OIII image from the UHC image using IRAF.

Photometry was done using the daophot package of IRAF in interactive mode. The procedure used was similar to the one outlined in Massey & Davis (1992). In this case image headers were edited to insert the right ascension and declination of the object as well as epoch (J2000) observation time and observatory. This allowed the IRAF airmass function to compute the relative air mass over the observatory site for each observation. Further a World Coordinate System (WCS) of right ascension and declination was imposed on each frame by providing the right ascension and declination of at least three stars in each frame. This was done to aid in positioning the synthetic aperture from image to image.

The daophot phot function was then used to perform synthetic aperture photometry on each image. The phot function computes the instrumental magnitude of the object as if viewed through a synthetic aperture of a specified radius of pixels. It does this by adding up the count inside the aperture. The sky background is then subtracted and the instrumental magnitude computed. Error in the magnitude is also computed based on the standard deviation of the sky background count (Davis 1994). Photometry was uncorrected for interstellar reddening and uncorrected for stellar contamination.

The diameter of the aperture for the comparison stars was determined by observing the point spread function of several stars (one shown in Figure 4). Based on this the aperture radius was set to 15 pixels. As recommended by Massey & Davis (1992), the sky annulus was set to 5 pixels beyond this at 5 pixels wide. Instrumental magnitudes on four stars in each frame for each object were obtained to provide a continuum reference between filters.

For the program objects a larger aperture was used. For the smaller objects such as NGC 7662, the aperture was set after examining a graph through the object as in Figure 5 so to encompass the whole object.

For larger objects such as NGC 598, several apertures were used to determine the instrumental magnitude of various parts of the larger object. The different parts in the larger objects were selected to coincide with visual features that had different colours in combined LRGB images to determine if the chemical make up of these regions was different. This was done on three objects, NGC 598, 650 and 6618. The location of these photometric measurements are shown in Figure 6.

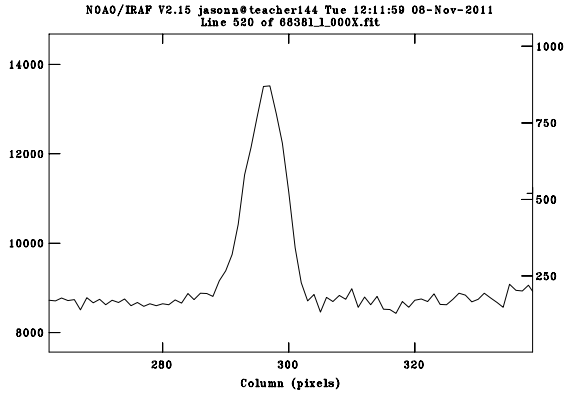


Fig. 4.— Stellar point source function

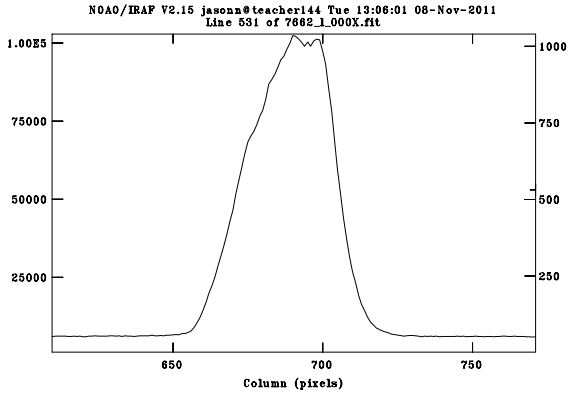


Fig. 5.— Extended object point source function

Once photometry was complete, various colour indexes were created to gage the brightness of the image in each band. A blue minus green (B-G) index was created as a comparison index. Indexes were created by subtracting the narrow band magnitude from the wide colour band that the narrow band was resident, so the indexes created were B-UHC, B-OIII and R-SII. Further a synthetic B-H $\beta$  was created by taking the magnitude of the image created by subtracting the OIII image from the UHC image then using that magnitude as H $\beta$ .

Once the colour indexes were generated, a method similar to that described by Birney et al (2008, p192) for the conversion of photometry data to a standard system was used to determine if a detection had been made. In this case the various narrow band indexes were plotted against the B-G index. For the continuum objects this created a line of points that standard linear regression could be used on to generate a best fit line. Qualitatively one can then check to see if a particular element line is present by checking to see how far

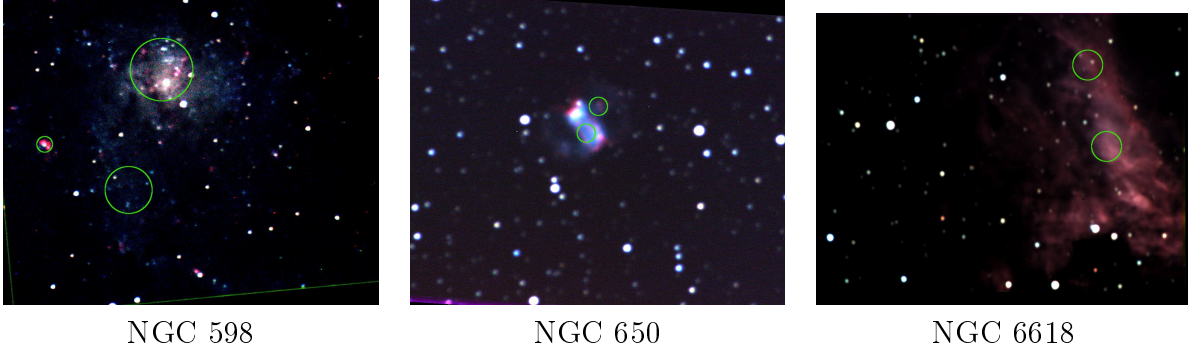
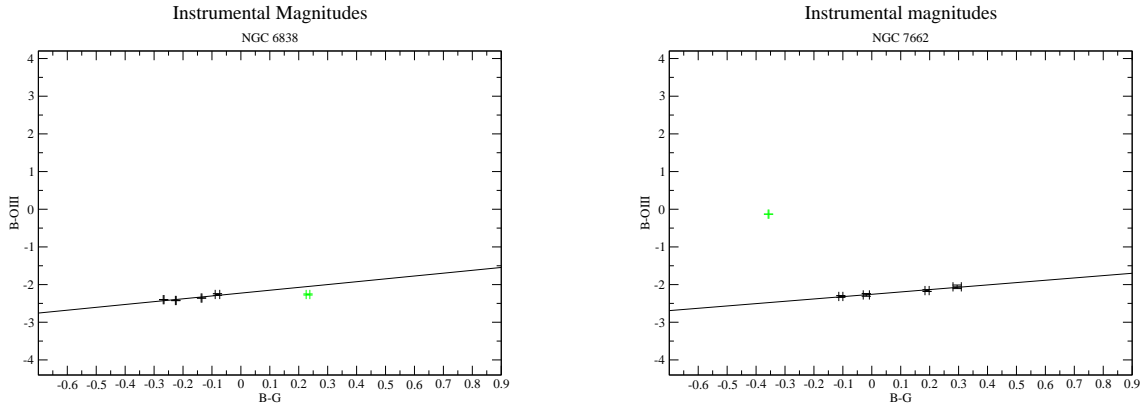


Fig. 6.— Location of photometric measurements

the plotted point for an object is near the regression line for that index. If the point is on or near the regression line then the change in magnitude caused by the narrow band filter on the object is similar to the change caused to the continuum objects in the field and would indicate that the particular emission/absorption line was not detected. Conversely if the plotted object point is not near or on the regression line, this would indicate that the elemental emission/absorption line was present. Figure 7 shows examples of both the non-detection of OIII in NGC 6838 and the positive detection of OIII in NGC 7664, the object in question being plotted in green with black points being the continuum objects in frame and the black line being the regression line of the continuum objects.



Negative detection for OIII in NGC 6838

Positive detection for OIII in NGC 7662

Fig. 7.— Graphical detection of lines

A quantitative approach to detection was performed by determining the distance from the regression line to the object point. This can be done if the equation of the regression line is put in the form of Equation 1:

$$ax + by + c = 0 \tag{1}$$

and then using Equation 2 (WolframWeb 2011) can find the distance to the line from the point.

$$d = \frac{|ax + by + c|}{\sqrt{a^2 + b^2}} \tag{2}$$

If the object’s index point is farther from the line than a certain value, it is likely that the emission/absorption line is present and thus the element is present. In this project this value was determined by taking twice the average of the standard deviations of the magnitude of the continuum stars for each filter. This gave a value of 0.48 as being the minimum distance from the regression line for a positive detection.

### 3. Results and Discussion

#### 3.1. Results

After image processing and photometry, the instrumental magnitude indexes in Table 3 were obtained.

Object	Index				
	B-G	B-UHC	B-OIII	B-Hβ	B-SII
NGC 185	-0.04±0.02	-0.52±0.02	-1.58±0.03	-0.68±0.02	-1.29±0.03
NGC 598 Core	-0.22±0.02	-0.76±0.02	-2.62±0.06	3.78±0.03	-1.52±0.03
NGC 598 Cloud (NGC 595)	-0.53±0.05	-0.58±0.04	-1.66±0.07	4.09±0.06	-1.63±0.05
NGC 598 Arm	-0.35±0.05	-1.68±0.12	-2.33±0.15	3.54±0.06	-0.13±0.10
NGC 650 Body	-0.27±0.01	0.07±0.01	-3.66±0.01	-1.01±0.01	-2.43±0.01
NGC 650 Lobe	-0.31±0.04	0.09±0.03	-2.34±0.03	-0.70±0.04	-2.44±0.02
NGC 6618 A	-0.31±0.03	0.30±0.03	-0.65±0.03	(1)	-4.25±0.10
NGC 6618 B	-0.35±0.02	-0.34±0.02	-1.35±0.03	-0.72±0.03	-3.40±0.09
NGC 6838	0.23±0.01	-0.32±0.01	-2.26±0.02	2.85±0.01	-2.33±0.01
NGC 7662	-0.36±0.01	0.00±0.01	-0.13±0.01	-1.20±0.01	0.78±0.01

Note:

(1) This part of NGC 6618 shifted to the edge of frame during registration and no measurement was possible.

Table 3: Obtained Instrumental Magnitude Indexes

These were plotted on graphs and the distance to the relevant regression line was computed using the method described above in section 2.4. These are shown in Table 4.

Object	Index			
	B-UHC	B-OIII	B-H $\beta$	B-SII
NGC 185	0.05	0.89	0.06	1.11
NGC 598 Core	0.13	0.00	0.48	0.58
NGC 598 Cloud (NGC 595)	0.48	0.58	0.91	0.33
NGC 598 Arm	0.34	0.16	0.42	1.75
NGC 650 Body	0.69	1.09	0.17	0.08
NGC 650 Lobe	0.73	0.22	0.38	0.09
NGC 6618 A	0.92	2.55	(1)	1.41
NGC 6618 B	0.66	1.96	0.55	0.56
NGC 6838	0.13	0.17	0.21	0.13
NGC 7662	0.67	2.00	1.42	3.02

Note:

(1) This part of NGC 6618 shifted to the edge of frame during registration and no measurement was possible.

Table 4: Object to regression line distances

Given a threshold distance of 0.48, the results on Table 4 would suggest positive detections of OIII in NGC 185, the molecular cloud in NGC 598, the main body of NGC 650, NGC 6618 and NGC 7662. Positive detection of H $\beta$  is suggested for the molecular cloud of NGC 598, portions of NGC 6618 and NGC 7662. SII detection is suggested in NGC 185, NGC 598 core and arm, NGC 6518 and NGC 7662. NGC 6838 did not show any indication beyond what would be expected from a continuum source.

### 3.2. Discussion

#### 3.2.1. Correlation of results with previous surveys

As seen in section 3.1 there were many positive indications of the presence of OIII, SII and H $\beta$  using this method. We now show that these indications are not spurious by looking at previous spectroscopic studies of these objects.

NGC 185 is a dwarf elliptical galaxy that is a companion to the nearby galaxy NGC 224 (M31) (Da Costa & Mould 1988). It is located at a distance of approximately 640 kpc from the Sun (NED 2011). It has been classified as a Seyfert galaxy due to its line emissions (Ho et al 1997) though recently some doubt has been cast on this (Martins et al 2011). A dust cloud is visible near the centre of this galaxy as seen in Figure 8. The Seyfert designation along with the visible dust cloud would suggest that there could be line emissions that could have been seen in this survey. As shown in Table 4, strong indications of OIII and SII were detected. H $\beta$  was shown to be near what would be expected for a

continuum object. This is consistent with the results of Ho et al (1997) as well as Marleau et al (2010).



Fig. 8.— Dust Cloud in NGC 185

NGC 598 (M33) is a spiral galaxy of the Local Group located approximately 884 kpc from the Sun (NED 2011) and is the farthest object in this survey. The large apparent size of NGC 598 allowed for the selection of three distinct areas to be studied. Shown in Figure 6, these areas were the core of the galaxy, a reddish cloud in one of the arms (NGC 595) and one of the spiral arms. These areas show different compositions. NGC 595 has indications of OIII and  $H\beta$  whereas the arm has no indication of this and the central bulge has a possibility of an indication of only the  $H\beta$  line. Conversely the core and arm show SII and none for NGC 595. The sulfur indication for all three is consistent with Comte & Monnet (1974). Crockett et al (2006) suggest that the gas near the core have more  $H\beta$  than OIII and these observations would tend to support that. The detection of OIII and  $H\beta$  in NGC 595 is also consistent with Kwitter & Aller (1981).

NGC 650 (M76) is a planetary nebula within our galaxy located about 746 pc from Earth (Stanghellini et al 2008), making it the closest object in this survey. As can be seen in Figure 6 the nebula consists of an optically dense bar shaped region from which two loop shaped lobes are attached. Filter photometry in this project on the bar shaped body indicated the presence of OIII but no indication of  $H\beta$  or SII. Photometry on the lobe observed did not give a positive indication of any of the three elements, though  $H\beta$  may be present as the measurement is close to the threshold set by this paper for detection. The observation for the core is generally consistent with spectroscopy from Kwitter & Henry (1996), Kaler (1980) and Henry et al (2004). Observations of the lobe don't seem to be consistent with the published observations. This may be due to the low observed brightness introducing error within the observations reported here, or the observations in the published data may not have specifically looked at the chemical abundances in the lobes.

NGC 6618 (M17) is an emission nebula with an associated open cluster located about 1.8kpc from Earth (Kharchenko et al 2005). These observations looked at two areas of the nebula, one more optically dense (6618A in Table 4) than the other and are shown in Figure 6. Due to the shifting that occurred while registering the UHC image with the OIII image in order to create the  $H\beta$  image, the location for measuring position 6618A was shifted too close to the edge of the frame to acquire a measurement for this region for  $H\beta$  so no value is given for this in Tables 3 and 4. For region 6618B, our observations indicate the presence of all three of OIII,  $H\beta$  and SII. OIII and SII are indicated by these observations for region 6618A. These observations are consistent with the observations presented in Peimbert et al (1992). Peimbert et al (1992) actually measured the same regions and the results presented here are consistent on a region by region basis as well.

NGC 6838 (M71) is a globular cluster located about 4 kpc from Earth (Harris 1996 2009). Being a globular cluster, it was expected that little if any interstellar gas would be present (Marks & Kroupa 2010) and that the detection profile would be consistent with the continuum stars. This was indeed the case for this object. This is consistent with other observations (Snedden et al 1994) which indicate a stellar spectral profile for the cluster. This makes NGC 6838 an important test of this technique in terms of testing for false positive indications.

The final object observed was the planetary nebula NGC 7662. This object is located about 790pc from Earth (Stanghellini et al 2008). The common name for this object, the Blue Snowball, and a cursory examination of the LRGB image of the nebula in Figure 9 shows that it has a blue-green colour suggesting plenty of OIII. The observations presented here do indicate the presence of OIII, but also the presence of  $H\beta$  as well as SII indicating a chemically rich nebula. This is consistent with the observations of Kaler (1980) and Henry et al (2004) for the presence of OIII, with the observations of Beck et al (1981) for  $H\beta$ , and with the observations of Kwitter et al (2003) for SII.

### 3.2.2. *Analysis of technique*

An examination of the strong correlation of the results of this survey and previously published results suggest that this technique of using wide and narrow band filters to detect specific elements through specific line emissions has merit. Given the proper set of wide and narrow band filters, an observer can determine with reasonable accuracy if, by the detection of it's emission line, a particular element species is present in an astronomical body. As shown above this works on a variety of object classes and at a variety of distances from a few hundred parsecs to intergalactic distances. The technique is simple and inexpensive to implement, especially if only looking for one particular species as two relatively inexpensive filters are all that are required: a narrow band filter for the emission line of the species in question and a wide band filter that encompasses the narrow band filter. At that point



Fig. 9.— NGC 7662 LRGB image

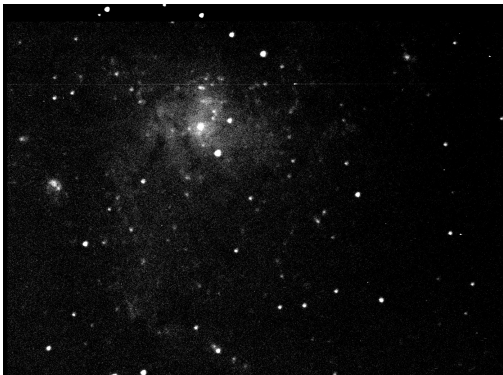
two simple observations with sufficient integration time to detect the object in the narrow band filter are really all that are needed. After standard image processing and synthetic aperture photometry with readily available software tools some simple mathematics is all that is required to determine if the element species is present.

This technique is suited as a compliment to standard spectroscopic techniques as attempting a complete spectrum with this technique would be more expensive than using a spectrometer. That being said, its usefulness for survey and discovery work is better than a spectrometer since a large area of the sky can be imaged and scanned at once. Every object in the field of view of the optical system/imaging system at the time of imaging can be tested in two observations. With a sufficiently large field of view, a large survey for a particular emission line can be completed relatively quickly. This means that not only does the survey take less time, but that less telescope time is needed to do the observations.

There is a limitation to this technique. If an object has considerable radial velocity, or is sufficiently distant that it has significant cosmological red shift the emission lines may be shifted out of the narrow band filter's bandpass. This would then provide a false negative for the particular element. Further sufficient shifting could move an unrelated emission line into the narrow filter's bandpass then providing a false positive indication. This limits the use of this technique to objects with lower radial velocities or galaxies that are close enough to our own as to not have significant cosmological red shift.

### 3.2.3. $H\beta$ filter synthesis

During the planning stages of this project, it was uncertain that the narrow band OIII and SII filters would arrive in time (a  $H\alpha$  filter was also supposed to be part of the filter set but had not arrived in time for observations) so observations were planned to be made with the wider UHC filter, covering not just the two blue-green OIII lines but the  $H\beta$  line as well. This would have allowed for a less complete test of the observation method as the UHC filter would indicate the presence of either or both of OIII and  $H\beta$ . Since the other narrow band filters had not yet arrived, observations with the UHC filter and wide band filters were started. Fortunately the OIII and SII filters did arrive part way through the observing program. Normally this would the UHC observations obsolete. It was during the observation of NGC 598 that the author noticed that the raw image from the CCD of the UHC filter quite clearly showed NGC598 while the raw image from the OIII filter barely showed anything at all as in Figure 10. It is important to note that the screen stretch for each image is different since it wasn't possible to see the OIII image at a stretch value that didn't wash out the UHC image. Since the reduction in flux between the two filters is not that great, the difference must have been due to strong  $H\beta$  emission and weaker OIII emission.



NGC 598 UHC filter image



NGC 598 OIII filter image

Fig. 10.— NGC 598 UHC and SII images

This triggered the author to think that if the OIII image was subtracted from the UHC image, what would be left would be the flux from the  $H\beta$  line. This provided a means to test for the  $H\beta$  line without a filter designed for that particular band in hand.  $H\beta$  frames were generated by registering the UHC and OIII images and then subtracting, pixel by pixel, the OIII image from the UHC image. This left an image that would appear as if taken with an  $H\beta$  filter, in essence synthesizing such a filter. As seen in section 3.2.1, this filter synthesis appears to produce results consistent with published observations of the  $H\beta$  line in the program objects.

### 3.2.4. Sources of error

No matter how carefully planned and executed, no observations are free of error. For this project there are several potential sources of error in the data. As there was slight mis-collimation of the secondary mirror in the telescope, stellar images were slightly misshapen compared to the circles with a fully collimated instrument. This may cause the algorithm that determines the instrumental magnitudes to miss some of the flux, lowering the measured magnitudes. This will have been mitigated by the notoriously bad seeing at the observing site, causing the misshapen stars to become circular again. Further, the point source function of the stars was examined and the aperture adjusted to accommodate the whole stellar image.

Errors related to the CCD are also present. Hot pixels, cosmic ray strikes and non-uniformity of the sensitivity across the CCD sensor all contribute to error. Mitigation of these errors was accomplished by the use of dark and flat frames and the (inadvertent) slight moving of the location of the image on the CCD from frame to frame for each filter.

The continuum comparison objects for each objects were four stars visible in each frame. It was attempted that the stars chosen were not known variables but due to the dim nature of many of the stars, it is possible that one or more of them are undiscovered variables. Having more than one comparison star helps to mitigate this possibility. Further for all objects other than NGC 6838 and NGC 7662 the series of observations was performed over a time frame of approximately 1.75 hours, removing errors from long term variability in any event. Observations of NGC 6838 and NGC 7662 were split over two separate nights due to the delay in obtaining the OIII and SII filters. Since all four stars for each of these objects lie practically on their respective regression lines, it is unlikely that any of those stars are variable over a time frame of a month.

Measurement error may have occurred as the aperture for each object and star was manually placed. Though the centering algorithm for the daophot package was used for the stars, ensuring the centring of the aperture, this was not possible for the program objects as all are extended objects with variable brightness across their area. To mitigate this a WCS was placed on each frame which allowed positioning of the aperture over the appropriate part of the object to within approximately 1 arc second.

Further measurement error will have come from stellar contamination from stars that may have fallen within the aperture, though attempts were made to avoid this. This should not be a major source of error as the comparison is between apertures over the same region, so any stars will be in the aperture in both frames for the comparison and hence cancel their effect out.

Sky subtraction will also be a cause of error as often the sky annulus around the magnitude aperture may contain stars or for large extended object, part of the object itself. Again as with stellar contamination this should not be a factor as the comparison is

between the same part of the sky each time.

#### 4. Conclusion

The technique described in this paper has merit for the detection of elements in astronomical objects without the use of spectroscopy. This can be done at considerable cost savings for both the amateur and professional astronomer as observations can be done with inexpensive filters. Often many amateur astronomers already possess some of these filters for use in combating light pollution further reducing cost.

Since only two relatively short sets of observations are needed, one for the narrow band line filter and one for the wide band filter that encompasses the narrow band, less telescope time may be required than with a spectrograph further reducing cost, especially for the professional astronomer.

Filter synthesis, where one slightly wider narrow band filter in combination with a narrower band filter is a viable technique for the detection of emission lines that are visible in the wider filter, but not the narrower filter. This can lower cost by preventing the need to purchase an additional filter.

The technique is simple in its implementation which allows for its easy use by amateur astronomers, providing them with another means of performing useful science as part of their hobby. The technique also uses tools most amateur astrophotographers already have in terms of imaging equipment and software. Depending on the imager and filter sets owned by the astrophotographer the additional investment in filters would likely be minimal.

Though simple and cost effective, this technique won't replace spectroscopy in the detailed analysis of chemical abundance in astronomical objects as a large supply of filters would be needed. Where this technique will excel is in surveys for specific elements where areas of the sky limited only by the field of view of the CCD can be checked with one set of observations.

#### 5. Acknowledgments

This research has made use of the SIMBAD database, operated at CDS, Strasbourg, France.

This research has made use of the NASA/IPAC Extragalactic Database (NED) which is operated by the Jet Propulsion Laboratory, California Institute of Technology, under contract with the National Aeronautics and Space Administration.

## REFERENCES

- Antares, 2008, Manufacturer supplied bandpass graph for UHC filter
- Beck, S.C., Lacy, J.H., Townes, C.H., Aller, L.H., Geballe, T.R. Baas, F., 1981, ApJ 249, 592
- Belikov, A.N. & Roser, S., 2008, A&A 489, 1107
- Birney, D.S., Gonzales, G., Oesper, D., 2008, Observational Astronomy (Cambridge)
- Caballero, D.L., 1947, JOSA 37, 176
- Cianci, S., Bland-Hawthorn, J., O’Byrn, J., 2004, in Optical Fabrication, Metrology, and Material Advancement for Telescopes, Atad-Ettedgui, E. & Dierickx, P. eds., SPIE 5495, 520
- Comte, G. & Monnet, G., 1974, A&A 33, 161
- Crockett, N.R., Garnett, D.R., Massey, P., Jacoby, G., 2006, ApJ 637, 741
- Davis, L.E., 1994, A Reference Guide to the IRAF/DAOPHOT Package (NOAO)
- Da Costa, G.S., & Mould, J.R., 1988, ApJ 334, 159
- Dickenson, T. & Dyer, A., 2002 The Backyard Astronomer’s Guide 2nd ed., (Richmond Hill:Firefly)
- Edwards, M.L., Bandyopadhyay, R.M., Eikenberry, S.S., Mikles, V.J., Moon, D.-S., 2010, in IAU Symp. 272, Active OB stars, Neiner, C., Wade, G., Meynet, G., Peters, G. eds, p 606
- Fabry, C., & Perot, A., 1901, ApJ 13, 265
- Freedman, R.A. & Kaufmann, W.J., 2007, Universe 8th ed. (New York: Freeman)
- Finkelman, I. & Brosch, N., 2011, MNRAS 413, 2621
- Forde, K.P., Butler, R.F., Peat, D., Golden, A., O’Tuairisg, S., 2005, SPIE 5823, 216
- Halliday, D. & Resnick, R., 1988, Fundamentals of Physics (New York:Wiley)
- Harris, W.E., 1996, AJ, 112, 1487
- Harris, W.E., 2009, mwgc.dat, <http://physwww.physics.mcmaster.ca/%7Eharris/mwgc.dat> (accessed 16 Nov 2011)
- Henry, R.B.C., Kwitter, K.B., Balick, B., 2004, AJ 127 2284

- Hyperweb, 2011a, Quantum processes, <http://hyperphysics.phy-astr.gsu.edu/hbase/mod5.html#c2> (accessed 17 Nov 2011)
- Hyperweb, 2011b, Hydrogen energies and spectrum, <http://hyperphysics.phy-astr.gsu.edu/hbase/hyde.html#c3> (accessed 17 Nov 2011)
- Ho, L.C., Filippenko, A.V., Sargent, W.L.W., 1997, *ApJS* 112, 315
- Johnson, H.L. 1955, *AnAp* 18, 292
- Johnson, W.W.A., 1939, *PAAS* 9, 262
- Kaler, J.B., 1980, *ApJ* 239, 77
- Kharchenko, N.V., Piskunov, A.E., Soser, S., Schilbach, E., Scholz, R.-D., 2005, *A&A* 438, 1163
- Kwitter, K.B. & Aller, L.H., 1981, *MNRAS* 195, 939
- Kwitter, K.B. & Henry, R.B.C., 1996, *ApJ* 473, 304
- Kwitter, K.B., Henry, R.B.C., Milingo, J.B., 2003, *PASP* 115, 80
- Lissberger, P.H., 1959, *JOSA* 49, 121
- Lissberger, P.H. & Wilcock, W.L., 1959, *JOSA* 49, 126
- Lofdahl, M.G., Henriques, V.M.J., Kiselman, D., 2011, *A&A* 533, A82
- Maitzen, H.M., 1976, *A&A* 51, 223
- Marks, M. & Kroupa, P., 2010, *MNRAS* 406, 2000
- Marleau, F.R., Noriega-Crespo, A., Misselt, K.A., 2010, *ApJ* 713, 992
- Martins, L.P., Lanfranchi, G., Goncalves, D.R., Magrini, L. Teodorescu, A.M., Quireza, C., 2011, [arXiv:1110.5891v1](https://arxiv.org/abs/1110.5891v1)
- Massey, P. & Davis, L.E., 1992, *A User's Guide to Stellar CCD Photometry with IRAF* (NOAO)
- Mees, C.E.K. & Wratten, S.H., 1906, *PA* 14, 572
- Nagao, T. et al, 2008, *ApJ* 680, 100
- NED, 2011, NASA/IPAC Extra Galactic Database, <http://ned.ipac.caltech.edu> (Accessed 13 Nov 2011)

- OptosigmaWeb, 2011, Filters & Apertures, <http://www.optosigma.com/products/optical-components/filters-apertures> (Accessed 17 Nov 2011)
- Orion Telescopes, 2009, LRGB Filter Set (Watsonville, CA:Orion Telescopes & Binoculars)
- Orion Telescopes, 2009a, Orion Extra Narrowband Oxygen-III Imaging Filter (Watsonville, CA:Orion Telescopes & Binoculars)
- Orion Telescopes, 2009b, Orion Extra Narrowband Sulfur-II Imaging Filter (Watsonville, CA:Orion Telescopes & Binoculars)
- Paunzen, E., Pintado, O.I., Maitzen, H.M., 2002, *A&A* 395, 823
- Peed, A.J. 1987, Transmission of Wratten Filters, in *CRC Handbook of Chemistry and Physics*, 1st Student Edition, Weast, R.C. ed. (Boca Raton, FL : CRC Press)
- Peimbert, M., Torres-Peimbert, S., Ruiz, M.T., 1994, *RMxAA* 24, 155
- Snedden, C., Kraft, R.P., Langer, G.E., Prosser, C.F., Shetrone, M.D., 1994, *AJ* 107, 1773
- Stanghellini, L., Shaw, R.A., Villaver, E., 2008, *ApJ* 689, 194
- ShelyakWeb, 2011, Shelyack Instruments, [http://www.shelyak.com/rubrique.php?id\\_rubrique=12](http://www.shelyak.com/rubrique.php?id_rubrique=12) (Accessed 12 September 2011)
- van Hubl, A., 1912, *PA* 20, 405
- Wallace, R.J., 1906, *ApJ* 24, 268
- Wallace, R.J., 1908, *ApJ* 27, 106
- WolframWeb, 2011, Point-Line Distance–2-Dimensional – from Wolfram MathWorld, <http://mathworld.wolfram.com/Point-LineDistance2-Dimensional.html> (Accessed 09 November 2011)